CrystEngComm

Accepted Manuscript

ROYAL SOCIETY OF CHEMISTRY

www.rsc.org/crystengcomm

Journal Name

RSCPublishing

ARTICLE

Mechanism of hydrogen treatment in $KTiOPO_4$ crystals at high temperature: Experimental and first-principles studies

Yang Zhang, Yanhua Leng, Jian Liu, Nianjing Ji, Xiulan Duan, Jing Li, Xian Zhao, Jiyang Wang,* Huaidong Jiang,*

Cite this: DOI:

Received ,
Accepted

DOI:

www.rsc.org/

Hydrogen annealing experiments on $KTiOPO_4$ (KTP) crystals with different temperatures, times and hydrogen concentrations were conducted in an atmospheric furnace. Theoretically, in order to analyze the reaction mechanisms of KTP under high temperature hydrogen annealing, the electronic structure, density of states and optical properties of stoichiometric KTP and KTP with different concentrations of oxygen vacancies and of OH were calculated from first-principles. In addition, various analysis methods were also used to study the mechanism of high temperature hydrogen annealing of KTP. The results show that oxygen ions diffuse from the interior to the surface under the conditions of high temperature and hypoxia. Since the high temperature provides enough energy for the chemical reaction, a number of the oxygen ions react with H_2 to produce H_2O, and a small portion are released in the form of O_2. As a result, oxygen vacancies are generated in the crystals, and a number of Ti^{4+} ions transform to Ti^{3+} for charge compensation. A correlation is established between the color (absorption intensity) of KTP after hydrogen annealing and the number of oxygen atoms removed. This work is helpful for better understanding the formation mechanism of gray tracks in KTP.

Introduction

The majority of nonlinear optical (NLO) materials currently used in optical devices are fabricated from bulk single crystals.[1] $KTiOPO_4$ (KTP), with outstanding NLO properties has been used in various applications,[2] especially in second harmonic conversion. However, the occurrence of laser damage caused by a defect referred to as "gray tracks" in KTP, has limited the use of this material in high-average-power laser systems.[3] Because the gray track defects absorb both the fundamental and second harmonic, continued operation after formation of the gray track may quickly lead to catastrophic failure.[4] The present study was initiated to determine the cause and possibly find a solution to this problem. The cause of gray tracks has been attributed to Ti^{3+} centers.[3-6] Ti^{3+} centers related to gray tracks can be produced by an electric field,[4] annealing in a hydrogen atmosphere,[6,7] x-ray irradiation,[8,9] or an intense laser beam.[10] To the best of our knowledge, no systematic studies on the reaction mechanism of hydrogen treatment at high temperature have been reported. This paper focuses mainly on experimental and theoretical studies of KTP annealing in a hydrogen atmosphere.

There are a large number of studies on the influence of high temperature hydrogen annealing for TiO_2, $Pb(Zr,Ti)O_3$ and $BaTiO_3$. Many theoretical models have been employed to explain the black coloration of titania under a H_2 flow, which include surface disorder,[11,12] oxygen vacancies (Ti^{3+} centers),[13-16] Ti-H,[11,17] and surface hydrogenation.[18] For instance, when $Pb(Zr,Ti)O_3$ thin films[19] and barium titanate (BTO) ceramics[20] are subjected to thermal treatment in H_2-N_2, hydrogen can enter into the lattice, bond with an apical oxygen ion, and degrade the ferroelectric properties of the material. It was observed that KTP subjected to 1 atm of hydrogen at 700-850 °C also developed a bluish-gray tint.[4] Hydrogen treatment of anatase single crystals results in the introduction of oxygen vacancies whose concentration can be varied by altering the processing temperature and hydrogen exposure time.[21]

In this paper, KTP annealing experiments with different temperatures, times, and hydrogen concentrations, which are three main factors influencing the experimental results, have been conducted in atmospheric furnaces. For the first time, we systematically studied the cause of coloration and oxygen vacancy formation (Ti^{3+} centers) in KTP after high temperature hydrogen annealing. The electronic structure, density of states and optical properties of KTP with different concentrations of oxygen vacancies and of OH have been calculated from first-principles. In addition, UV-visible absorption spectra, electron paramagnetic resonance (EPR) spectra, room temperature FTIR and Raman spectra, and the in situ infrared spectra were measured. Also, H_2-temperature programmed desorption (H_2-TPD), H_2-temperature-programmed reduction mass spectrometry (H_2-TPR-MS), and secondary ion mass spectroscopy (SIMS) measurements were carried out to attempt to explain the complex mechanism.

Experimental Procedure

Computational details

Calculations were performed with the plane-wave pseudopotential method implemented in the CASTEP package[22] with density functional theory (DFT), using the gradient-corrected Perdew-Burke-Ernzerhof (PBE) method. The ion-electron interaction was modeled by ultrasoft Vanderbilt-type pseudopotentials.[23] The presence of oxygen vacancies and hydroxylated KTP crystals in one unit cell with 64 ions were modeled by removing oxygen ions and by adding hydrogen ions bonding with oxygen ions, respectively. We considered both OH and oxygen vacancy concentrations of 1.56%, 3.12%, and 4.68%. The electronic band structure, density of states (DOS) and optical absorption spectra were calculated from the optimal geometry. Brillouin-zone integrations were made using a (2×2×2) k-point mesh following the Monkhorst–Pack scheme.[24]

Characterization

Hydrogen annealing experiments were carried out in an atmospheric furnace at different temperatures, times and hydrogen concentrations. The UV-visible absorption spectra were obtained with a UV-Vis absorption spectrometer operating in the 300-3000 nm wavelength region. The weak absorption peaks at 532 nm and 1064 nm were measured with a Photothermal Common-path Interferometer (PCI) and a laser calorimeter set-up by Stanford University.[25] EPR spectra were recorded on a Bruker EMX 10/12 spectrometer. The infrared spectrum was measured in situ using a Nicolet 6700 FTIR spectrometer with a resolution of 4 cm^{-1} in an atmosphere of hydrogen. SIMS was measured with a Model 2100 Trift II TOF-SIMS.

The H_2-temperature programmed desorption and H_2-temperature programmed reduction measurements were performed on a CPB-1-TPR (Quantachrome, U.S.) utilizing hydrogen as the reducing agent. Prior to the TPR measurements, samples were pretreated at 300 °C for 40 min in flowing He (50 mL/min) to remove moisture and impurities. After cooling the reactor to room temperature, a 10 mol% H_2-Ar (50 mL/min) gas mixture was introduced into the system. The sample was heated to 950 °C at a rate of 10 °C/min, and hydrogen consumption and the product gases during reduction were monitored using an AMETEK (LC-D-200 Dycor AMETEK) mass spectrometer.

Results and Discussion

The crystal structure of KTP is shown in Fig. 1. The structure contains helical chains consisting of TiO_6 octahedra that are linked at the corners and are separated by PO_4 tetrahedra. There are ten types of oxygen sites in KTP, and they can be divided into two groups: those in Ti-O-P chains consisting of O(1)-O(8) and those in Ti-O-Ti chains with short Ti-O bonds consisting of O(Ti1) and O(Ti2).[26] In previous study, oxygen vacancies can be generated by hydrogen reduction in TiO_2. It was reported that hydrogen is interstitially coupled to oxygen and forms OH under hydrogen annealing in Pb(Zr, Ti)O_3.[19,27] So we consider oxygen vacancies from different oxygen sites (see Fig. 1 and Fig. S1 in ESI†) and OH by adding hydrogen bonding at the different oxygen sites (see Figs. S6 and S8 in ESI†). In order to construct the structure models with different vacancies in one unit and to analyse the relationship between vacancy concentration and optical absorption, the concentrations of oxygen vacancies and of OH used in the calculations are 1.56%, 3.12%, and 4.68%.

The energy band structure, the total density of states (TDOS) and the partial density of states (PDOS) in KTP with oxygen vacancies at O(Ti1)+O(Ti2) were firstly calculated (Figs. S2, S3 and S4, ESI†). From the calculated results, the conditions of hydroxylated KTP and having oxygen ions removed only from O(Ti1) and O(Ti2) are not in accord with the experimental results, and the optical absorption does not depend on increasing the oxygen vacancy or OH concentration (see Fig. S5, S7 and S9, ESI†). On the other hand, the calculated results on oxygen ions removed from O(1) to O(8) are in good agreement with the experimental results. The formation energy of one oxygen vacancy plus the addition of one hydrogen atom can be denoted as:

$$E_1=E_{def}-(E_{per}-E_O) \quad (1)$$

$$E_2=E_{def}-(E_{per}+E_H) \quad (2)$$

where E_{def} is the total energy of the unit cell with defects, E_{per} is the total energy of the perfect lattice, and E_O and E_H are the energies of single O and H atoms, respectively. The formation energies of O_2 and H_2 molecules were firstly calculated, and then half of the energies were treated as the formation energies of single O and H atoms. Based on formula (1), the formation energy of oxygen ions at O(1)-O(8) and O(Ti1)+O(Ti2) are 5.217 and 6.293 eV, respectively. The formation energy of an oxygen vacancy at O(1)-O(8) is lower than that at O(Ti1)+O(Ti2), which indicates that the defect structure with an oxygen vacancy at O(1) to O(8) is more stable and easier to form. The calculated formation energies of adding a H atom to the lattice are 1.076 (adding a H atom bonding with O(1)-O(8)) and 1.007 eV (adding a H atom bonding with O(Ti1)+O(Ti2)). The positive formation energy means that H will not be absorbed by KTP and forms OH. Therefore, we discuss only the condition of oxygen atoms removal from O(1)-O(8) below.

As shown in Fig. 1, O atoms 1, 2 and 3 represent different O atoms from O(1) to O(8). To discuss the oxygen vacancy in KTP, we consider different oxygen vacancy concentrations: one oxygen vacancy, two oxygen vacancies and three oxygen vacancies in one unit cell that are removed from: a.) O ion 1, b.) O ions 1 and 2, and c.) O ions 1, 2 and 3.

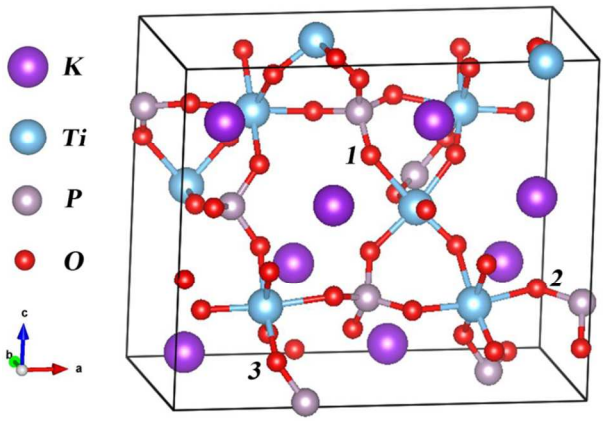

Fig. 1 View of KTP structure along the *b*-axis. The numerals 1, 2 and 3 indicate three different oxygen ions from O(1)-O(8).

The electronic band structure of stoichiometric KTP is shown in Fig. 2a. A band gap of about 3.11 eV at the zone center is obtained, which is 0.43 eV smaller than what is found from optical measurements (3.54 eV).[28] So scissor operators of 0.43 eV in energy are used in all the calculations below. The zero point is located at the top of the VB. The bottom of the CB and the top of the VB are very flat. A missing oxygen ion from the bulk or from the surface results in the localization of one or two electrons at an oxygen vacancy state.[29] A change in the distribution of the O^{2-} electron cloud has a direct effect on the electronic structure of KTP by forming a donor level below the CB,[30] as shown in Fig. 2b. It is very interesting that the concentration of oxygen vacancies is connected with the number of oxygen vacancy states. When two or three oxygen atoms removed from O(1) to O(8) in a unit, there are two or three states emerging between the VB and CB. The calculated energy band structure, DOS and PDOS of two and three oxygen vacancies from O(1) to O(8) are shown in Figs. S10, S11 in ESI†. Here, we show only the band structure for one oxygen vacancy from O(1)-O(8) in a cell. The oxygen vacancy state energy is 1.21eV (corresponding to 1025 nm) above the top of VB, which leads to increasing optical absorption at the visible and near-infrared wavelengths. By contrast, the oxygen vacancy state in TiO_2 is determined to be located 2.02–2.45 eV above the valence band, which corresponds to a wavelength of 506–614 nm.[31]

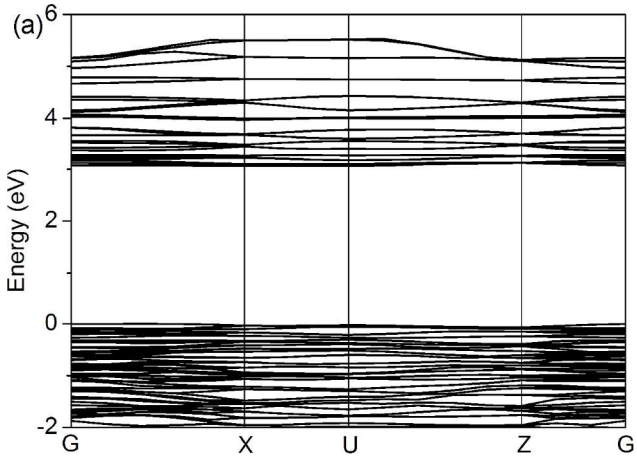

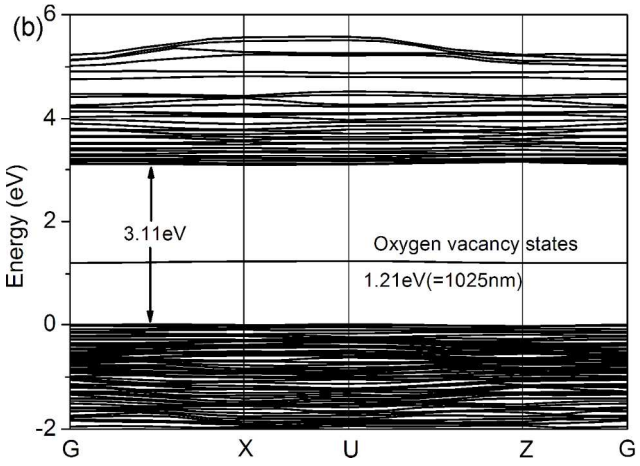

Fig. 2 The energy band structure of (a) stoichiometric KTP (b) KTP with one oxygen vacancy from O(1)-O(8) in a unit cell.

The total density of states (TDOS) and the partial density of states (PDOS) of stoichiometric KTP and KTP with one oxygen vacancy from O(1) to O(8) in a unit cell are shown in Figs. 3a and 3b, respectively. The Ti 4s and 3p states are located at a much lower energy of about -56 and -33 eV (not shown), respectively, and do not participate in the bonding between Ti and O. The fact that K orbitals have little influence on the electronic states of the other types of ions demonstrates that they form very weak bonds with neighbouring ions.[32] The Ti ions are highly ionized in the CB, and the PDOS in the VB region shows that the Ti-O bond is partially covalent. The sharp peaks of the P 3s and 3p states around -20 eV and -17 eV show a strong admixture with the O 2s orbitals in forming the tetrahedral bonding in PO_4. The strong interaction at -16 eV between O(Ti1)+O(Ti2) indicates that this type of O ion bonds only with Ti ions. The DOS of KTP with one oxygen vacancy in a unit cell is similar to that of stoichiometric KTP, but an oxygen vacancy state between the CB and VB emerges, which alters the band structure somewhat. As the oxygen vacancy is moved from O(1) to O(8) in bonding with P atoms, a state at -18 eV also emerges among the P and the O(1) to O(8) ions.

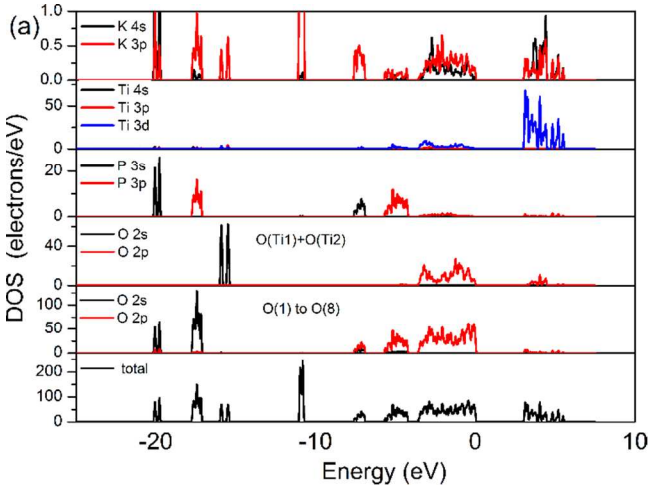

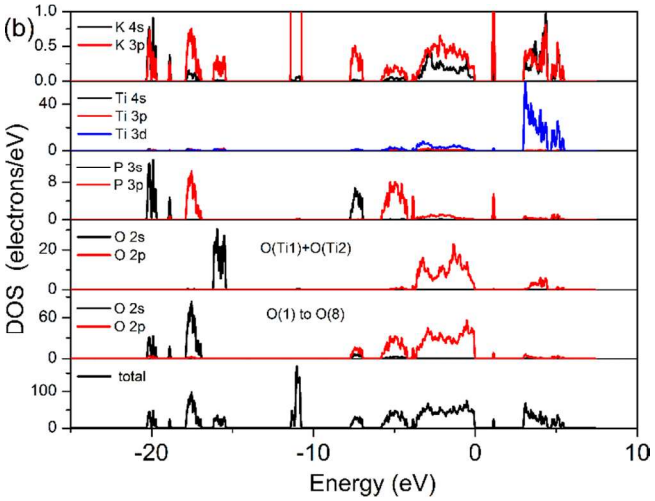

Fig. 3 The total density of states (TDOS) and the partial density of states (PDOS) in (a) stoichiometric KTP (b) KTP with one oxygen vacancy from O(1)-O(8) in a unit cell.

High temperature hydrogen annealing of KTP was conducted at temperatures of 200 °C, 400 °C, 600 °C, 800 °C, and 950 °C for 4 hours with a flow of 12.5 mol% H_2-N_2 gas mixture. All samples used were from the same KTP crystal, which was grown in a flux of $K_6P_4O_{13}$ and PbO, and then cut to a size of 4×4×1 mm^3. After annealing, the crystals were polished. A photograph of the samples annealed at the different temperatures is shown in the top half of Fig. 4b. X-ray powder diffraction before and after H_2 annealing at 950 °C was analyzed, and the results show that the process of annealing does not induce a phase transition. All the peaks in evidence can be indexed to a phase of KTP (JCPDS card no. 70-2073) (see Fig. S12, ESI†). The KTP crystals turned from a highly transparent state to gradually darker ones with increasing heat treatment temperature. In fact, the crystal surface began to turn gray at 400 °C, but the gray color disappeared after polishing. So the annealing process at 200 °C and 400 °C had little influence on optical absorption. Color change was reversible during re-annealing in an oxidizing atmosphere at high temperature. In addition to annealing temperature, the influence of annealing time and hydrogen concentration were also studied (Figs. S12 and S13, ESI†). The temperature was fixed at 600 °C, and only when the annealing time was long enough or the hydrogen concentration was high enough, were the color change and absorption increase obvious. We compared the calculated results on absorption with the experimental absorption spectra (see Figs. 4a and 4b). The calculated results showed that the absorption in the visible and near-infrared region increased with oxygen vacancy concentration increase, and the experimental absorption spectra showed that the absorption intensity increased with increasing annealing temperature, as predicted in the calculated results. The absorption increased with increasing annealing temperature because oxygen vacancies are easier to form at high temperatures. Thus, we conclude that temperature is the primary factor that leads to the color change and the increasing optical absorption, based on our experiments. To maintain charge balance, some Ti^{4+} ions are transformed to Ti^{3+}. The black coloration partially results from the transitions (Ti^{3+} $3d^1$→Ti^{3+} $3d^1$ or Ti^{4+} $3d^0$) of the Ti^{3+} $3d^1$ electrons to the unoccupied Ti 3d states.[33]

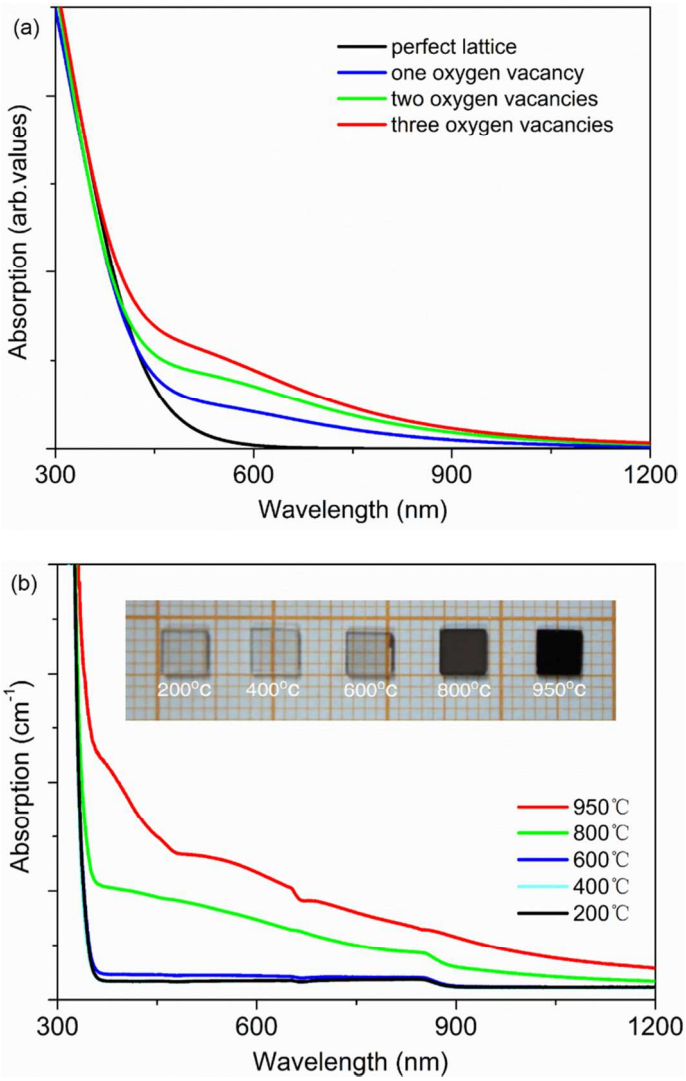

Fig. 4 (a) Calculated absorption spectra of KTP with different oxygen vacancy concentrations from O(1) to O(8). (b) Experimental absorption spectra at different temperatures. The illustration on the top of Fig. 4(b) shows photographs of KTP crystals annealed in H_2 gas at different temperatures.

Previous study reported that bulk oxygen defects in TiO_2 can readily serve as color centers causing absorption and making TiO_2 more active at visible wavelengths.[34] The formation of the defects in a hydrogen atmosphere at high temperature may be described by the following defect equilibrium equation[35]:

$$Ti^{4+}\text{-}O\text{-}Ti^{4+}+H_2 \rightarrow Ti^{3+}\text{-}V_O\text{-}Ti^{3+}+H_2O$$

At higher temperatures this equilibrium shifts to the right, which causes the concentrations of oxygen vacancy and Ti^{3+} increase. To determine the existence of Ti^{3+}, which indirectly reflects the emergence of Vo in KTP after annealing, the low temperature EPR spectrum at 77 K was recorded and shown in Fig. 5. The magnetic

field was parallel to the *c*-axis of the KTP crystal, and the microwave frequency was 9.3759 GHz. We also measured the EPR spectrum of unannealed KTP for comparison, and there was no Ti^{3+} signal. In contrast, the Ti^{3+} signals with a central g-value of 1.918 were quite apparent in the crystal after hydrogen annealing. Except for a different orientation of magnetic field, this is the same center described in an earlier EPR study.[6,9] The electrons remaining in the vacancy move towards the neighboring Ti atoms, forming reduced Ti^{3+} cations. In addition, the weak absorption at 532 nm and 1064 nm increased enormously to about three hundred thousand ppm·cm^{-1} after hydrogen annealing at 800 °C in stark contrast to the values of 3000 ppm·cm^{-1} and 30 ppm·cm^{-1} before annealing. These results also demonstrated that a number of Ti^{3+}-V_O color centers were produced after hydrogen annealing.

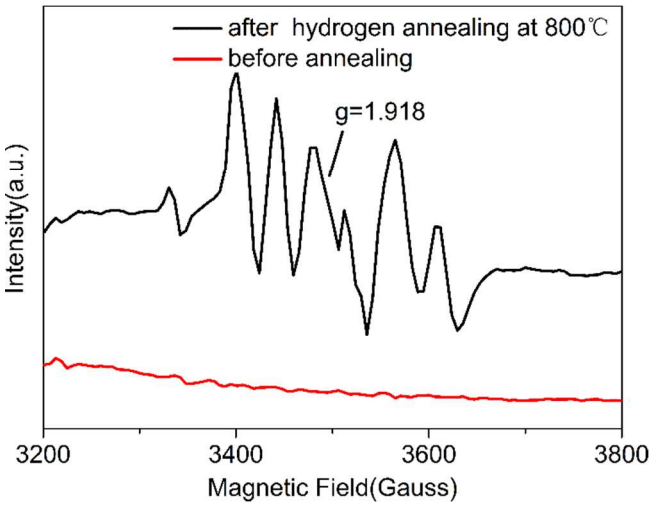

Fig. 5 EPR spectra of KTP with magnetic field parallel to the *c*-axis at 77 K.

To further confirm that it is oxygen vacancy (Ti^{3+} centers) and not OH that is produced during the process of annealing, and to study the formation process of oxygen vacancy, a further series of experiments were performed. The IR absorption spectrum can reflect the existence of OH after hydrogen annealing at high temperature.[36] However, we did not detect OH using both room temperature IR and Raman spectra measurements (see Figs. S15 and S16, ESI†). The in situ infrared spectrum in a hydrogen atmosphere at 500 °C was also measured to study the possibility of OH occurrence at high temperature. As shown in Fig. 6, the OH band was not detected in KTP before annealing. When the sample was heated to 500 °C in a hydrogen atmosphere, OH absorption peaks emerge, but the peak intensity is very weak. The detected OH arises from H_2O, which is produced in the reaction based on the above mentioned.

To further study the reaction mechanism of KTP crystal and H_2 at high temperature, H_2-TPD and H_2-TPR-MS were measured and analyzed. The H_2-TPD results show that KTP has no H_2 absorption at high temperature (Fig. S17, ESI†). In previous studies, the H_2-TPR profiles of ceria exhibit two peaks, the first one at about 500 °C corresponds to the reduction of surface-capping oxygen, while the second one, at a temperature above 800 °C, corresponds to bulk reduction.[37,38] However, in comparison to ceria, the H_2-TPR profile of KTP shows that there are no peaks corresponding to reduction and the consumption of hydrogen begins to increase suddenly above 600 °C. The increase does not cease until 950 °C, which means that KTP is being reduced beginning around 600 °C, and the reduction ratio keeps increasing with increasing temperature (Fig. S18, ESI†).

The hydrogen consumption and gas production during the reduction process of KTP were monitored using a mass spectrometer, and the results are shown in Fig. 7. The pre-treatment time is 40 min. The program begins at 32 °C and heats up at a rate of 1 °C/min. The sudden onset of the MS signal occurs at a temperature of about 600 °C in agreement with the TPR results. When H_2 consumption began, O_2 and H_2O were produced. The KTP crystal is the only oxygen source, so the elemental O in O_2 and H_2O can only come from the KTP. Under high temperature and hypoxic conditions, the oxygen ions in KTP diffuse from the interior to the surface, and the high temperature provides enough energy for the chemical reaction. From the mass spectroscopy results shown in Fig. 7, it is evident that most of the oxygen atoms on the surface react with H_2 to produce H_2O and a small portion releases in the form of O_2. Oxygen vacancies emerge due to the diffusion process, and some Ti^{4+} ions change to Ti^{3+} ions to balance the charge. In addition, SIMS with a sensitivity of ppb was also used to qualitatively detect the existence of OH. Although the sensitivity of SIMS is very high, it is difficult to obtain precise quantitative analysis. As shown in Fig. S19 in ESI†, the OH exists in KTP and exhibits no variation with depth. The extremely small amount of OH, which cannot be detected by IR and Raman spectra, may be due to the growth process of KTP but not to the annealing process, and will not induce enhanced optical absorption. We therefore conclude that, unlike $BaTiO_3$[39] and its isologues[36], the color variation and increasing optical absorption of KTP at visible and near infrared wavelengths are not caused by OH. Based on the comprehensive analysis of all above experimental results combined with the calculations, the coloration and the absorption increase of KTP after hydrogen annealing are due to oxygen vacancies.

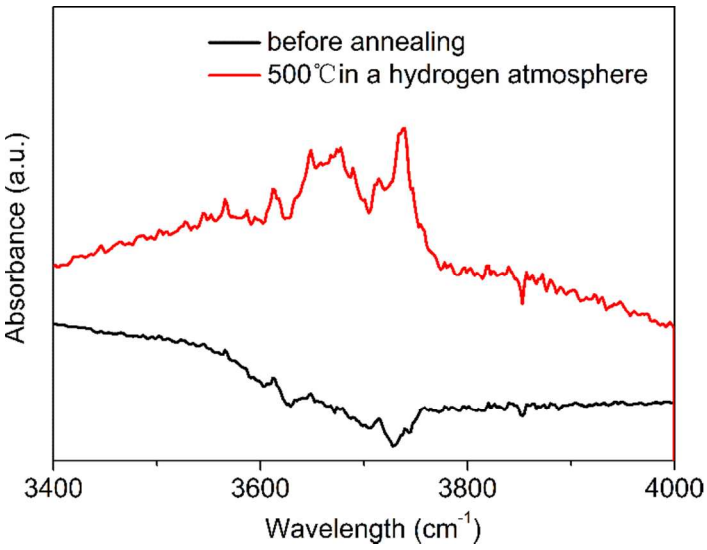

Fig. 6 In situ FTIR of KTP before heating, and at 500 °C in a hydrogen atmosphere.

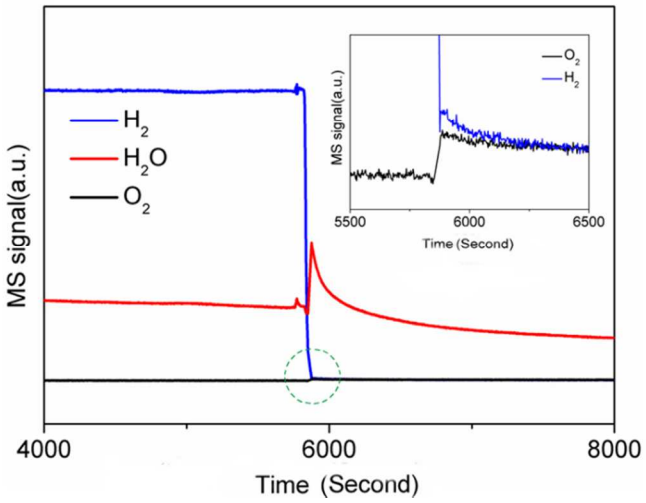

Fig. 7 Mass spectroscopy results vs. time for reduction process of KTP. The inset is a magnification of the circled region.

Conclusion

In summary, the reduction mechanism of KTP in an H_2 atmosphere at high temperature was investigated in detail. The results of both calculation and experiment show that it is oxygen vacancies (or Ti^{3+} centers) and not OH that produces the color change and increasing optical absorption. The oxygen vacancy concentration is mainly determined by the annealing temperature in comparison to the annealing time and the concentration of H_2. The oxygen vacancies are located from O(1) to O(8). At high temperatures and low oxygen environments, oxygen ions diffuse from the interior to the surface. Most of the oxygen ions on the surface react with H_2 to produce H_2O, and a small portion releases in the form of O_2. The oxygen vacancies then appear in the crystal and some Ti^{4+} ions transform to Ti^{3+} to ensure charge balance. After hydrogen annealing, the absorption at 532 and 1064 nm increases enormously and this is fatal for any putative application. This work will enable us to obtain a better understanding of gray track formation and provide important design principles for crystal engineering.

Acknowledgements

We thank Prof. R. Boughton for revising the manuscript. This work was supported by the National Natural Science Foundation of China (31430031, U1332118, 51172130, 51272130), the National Science Foundation of Shandong Province (JQ201117), and the Program for New Century Excellent Talents (NCET-11-0304).

Notes and references

[a]State Key Laboratory of Crystal Materials, Shandong University, 27 Shandanan Road, Jinan, 250100, China. E-mail: hdjiang@sdu.edu.cn

† Electronic Supplementary Information (ESI) available: [details of any supplementary information available should be included here]. See DOI:

[1] M.E. Hagerman, K.R. Poeppelmeier, *Chem. Mater.*, 1995, **7**, 602-621.
[2] G.D. Stucky, M.L. Phillips, T.E. Gier, *Chem. Mater.*, 1989, **1**, 492-509.
[3] G. Loiacono, D. Loiacono, T. McGee, M. Babb, *J. Appl. Phys.*, 1992, **72**, 2705-2712.
[4] M.G. Roelofs, *J. Appl. Phys.*, 1989, **65**, 4976-4982.
[5] M. Scripsick, G. Edwards, L. Halliburton, R. Belt, *J. Appl. Phys.*, 1991, **70**, 2991-2994.
[6] M. Scripsick, G. Edwards, L. Halliburton, R. Belt, G. Loiacono, *J. Appl. Phys.*, 1994, **76**, 773-776.
[7] G. Loiacono, D. Loiacono, J. Zola, R. Stolzenberger, T. McGee, R. Norwood, *Appl. Phys. Lett.*, 1992, **61**, 895-897.
[8] B.V. Andreev, V.N. Efimov, *Mod. Phys. Lett. B*, 1992, **6**, 177-181.
[9] M. Scripsick, D. Loiacono, J. Rottenberg, S. Goellner, L. Halliburton, F. Hopkins, *Appl. Phys. Lett.*, 1995, **66**, 3428-3430.
[10] B. Andreev, V.A. Maslov, B. Mikhailov, S. Pak, O. Shaunin, I.A. Shcherbakov, *Proc. SPIE* , 1992, **280**, 280-289.
[11] F. Teng, M. Li, C. Gao, G. Zhang, P. Zhang, Y. Wang, L. Chen, E. Xie, *Applied Catalysis B: Environmental*, 2014, **148**, 339-343.
[12] X. Chen, L. Liu, Y.Y. Peter, S.S. Mao, *Science*, 2011, **331**, 746-750.
[13] D. Cronemeyer, *Physical Review*, 1959, **113**, 1222.
[14] E. Finazzi, C. Di Valentin, G. Pacchioni, *J. Phys. Chem. C*, 2009, **113**, 3382-3385.
[15] E. Finazzi, C. Di Valentin, G. Pacchioni, A. Selloni, *J. Chem. Phys.*, 2008, **129**, 154113.
[16] A. Naldoni, M. Allieta, S. Santangelo, M. Marelli, F. Fabbri, S. Cappelli, C.L. Bianchi, R. Psaro, V. Dal Santo, *J. Am. Chem. Soc.*, 2012, **134**, 7600-7603.
[17] Z. Wang, C. Yang, T. Lin, H. Yin, P. Chen, D. Wan, F. Xu, F. Huang, J. Lin, X. Xie, *Adv. Funct. Mater.*, 2013, **23**, 5444-5450.
[18] W. Wei, N. Yaru, L. Chunhua, X. Zhongzi, *RSC Adv.*, 2012, **2**, 8286-8288.
[19] S. Aggarwal, S. Perusse, C. Tipton, R. Ramesh, H. Drew, T. Venkatesan, D. Romero, V. Podobedov, A. Weber, *Appl. Phys. Lett.*, 1998, **73**, 1973-1975.
[20] W.P. Chen, X.P. Jiang, Y. Wang, Z. Peng, H.L.W. Chan, *J. Am. Chem. Soc.*, 2003, **86**, 735-737.
[21] Z. Lin, A. Orlov, R.M. Lambert, M.C. Payne, *J. Phys. Chem. B*, 2005, **109**, 20948-20952.
[22] M.C. Payne, M.P. Teter, D.C. Allan, T. Arias, J. Joannopoulos, *Rev. Mod. Phys.*, 1992, **64**, 1045-1097.
[23] D. Vanderbilt, Soft self-consistent pseudopotentials in a generalized eigenvalue formalism, *Phys. Rev. B*, 1990, **41**, 7892.
[24] H.J. Monkhorst, J.D. Pack, *Phys. Rev. B*, 1976, **13**, 5188-5192.
[25] A.L. Alexandrovski, G. Foulon, L.E. Myers, R.K. Route, M.M. Fejer, *Proc. SPIE*, 1999, **3610**, 44-51.
[26] W. Ching, Y.N. Xu, *Phys. Rev. B*, 1991, **44**, 5332-5335.
[27] H.J. Joo, S.H. Lee, J.P. Kim, M.K. Ryu, M.S. Jang, *Ferroelectrics*, 2002, **272**, 149-154.
[28] M. Sheik-Bahae, D.C. Hutchings, D.J. Hagan, E.W. Van Stryland, *IEEE J. Quantum Elect.*, 1991, **27**, 1296-1309.
[29] X. Pan, M.Q. Yang, X. Fu, N. Zhang, Y.J. Xu, *Nanoscale*, 2013, **5**, 3601-3614.
[30] H. Li, F. Zhou, Y.L. Lam, C.H. Kim, Mater. Res. Bull., 1999, **34**, 827-834.
[31] I. Nakamura, N. Negishi, S. Kutsuna, T. Ihara, S. Sugihara, K. Takeuchi, *Journal of Molecular Catalysis A: Chemical*, 2000, **161**, 205-212.
[32] V.V. Atuchin, V.G. Kesler, G. Meng, Z.S. Lin, *Journal of Physics. Condensed Matter*, 2012, **24**, 405503.
[33] F. Zuo, K. Bozhilov, R.J. Dillon, L. Wang, P. Smith, X. Zhao, C. Bardeen, P. Feng, *Angewandte Chemie*, 2012, **124**, 6327-6330.
[34] I.N. Martyanov, S. Uma, S. Rodrigues, K.J. Klabunde, *Chem. Commun.*, 2004, 2476-2477.
[35] J. Strunk, W.C. Vining, A.T. Bell, *J. Phys. Chem. C*, 2010, 114, 16937-16945.
[36] G.C. Yi, B.A. Block, B.W. Wessels, *Appl. Phys. Lett.*, 1997, **71**, 327-329.
[37] H. Yao, Y.F. Yao, Journal of Catalysis, 1984, **86**, 254-265.
[38] F. Giordano, A. Trovarelli, C. de Leitenburg, M. Giona, *J. Catal.*, 2000, **193**, 273-282.
[39] M. Wu, H. Huang, B. Jiang, W. Chu, Y. Su, J. Li, L. Qiao, *J. Mater. Sci.*, 2009, **44**, 5768-5772.

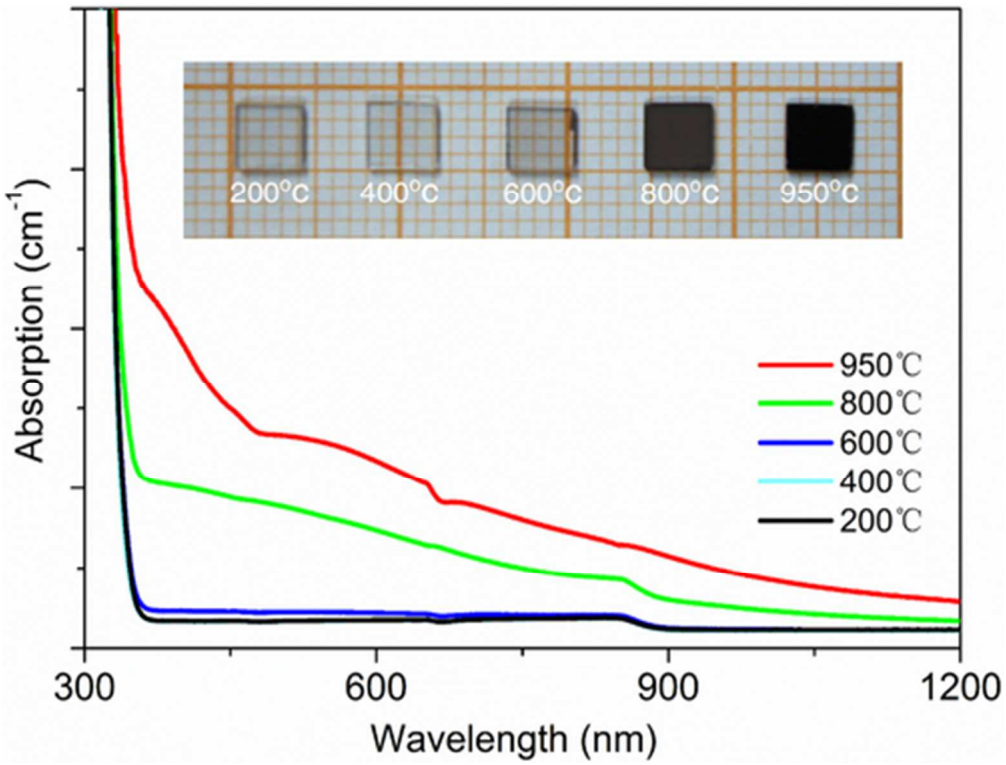

The mechanism of coloration and oxygen vacancy formation in KTP crystals treated by hydrogen annealing was systematically investigated.
42x32mm (300 x 300 DPI)